ELSEVIER

Biochimica et Biophysica Acta 1466 (2000) 205–220

BIOCHIMICA ET BIOPHYSICA ACTA
BBA

www.elsevier.com/locate/bba

Selective targeting of immunoliposomal doxorubicin against human multiple myeloma in vitro and ex vivo

Daniel E. Lopes de Menezes [a,1], Linda M. Pilarski [b], Andrew R. Belch [b], Theresa M. Allen [a,*]

[a] *Department of Pharmacology, University of Alberta, 9-70 Medical Sciences Bldg., Edmonton, Alta., Canada, T6G 2H7*
[b] *Department of Oncology, Cross Cancer Institute, University of Alberta, Edmonton, Alta., Canada, T6G 1Z2*

Received 13 December 1999; received in revised form 9 March 2000; accepted 14 March 2000

Abstract

Circulating malignant $CD19^+$ B cells have been implicated in the pathogenesis and relapse of multiple myeloma (MM). This study investigated the therapeutic applicability of using long-circulating liposome-encapsulated doxorubicin (DXR) targeted against the internalizing CD19 antigens present on human MM cells. In vitro binding studies using the $CD19^+$ MM cell line ARH77 demonstrated that CD19-directed immunoliposomes (SIL[anti-CD19]) specifically attached to these cells. Formulations of immunoliposomal doxorubicin (DXR-SIL[anti-CD19]) showed a higher association with, and higher cytotoxicity against, ARH77 cells than did non-targeted liposomal doxorubicin (DXR-SL) or isotype-matched controls (DXR-NSIL[IgG2a]). By using the pH-sensitive fluorophore, 1-hydroxypyrene-3,6,8-trisulfonic acid, binding of SIL[anti-CD19] to CD19 antigens was shown to trigger receptor-mediated internalization of the antibody–antigen complexes into endosomes. Targeting of SIL[anti-CD19] to $CD19^+$ B cells was also demonstrated in a heterogeneous mixture of peripheral blood mononuclear cells (PBMC) from MM patients. A decrease in cellular DNA (which is an indicator of apoptosis) caused by the cytotoxicity of DXR-SIL[anti-CD19] to myeloma PBMC was determined by using flow cytometry. While PBMC treatment with free DXR resulted in non-specific cytotoxicity to both B and T cells, DXR-SL were only minimally cytotoxic to either. In contrast, DXR-SIL[anti-CD19] were selectively cytotoxic for B cells in PBMC, indicating that this treatment may be effective in eliminating circulating malignant B cells in MM patients.

Keywords: Liposome; CD19; Doxorubicin; Targeted drug delivery; Multiple myeloma

Abbreviations: CHOL, cholesterol; Crbc, chicken red blood cells; DAPI, 4,6-diamidino-2-phenylindole; DXR, doxorubicin; DSPE, distearoyl phosphatidylethanolamine; FBS, fetal bovine serum; FITC, fluorescein isothiocyanate; [^{3}H]CHE, cholesteryl-[1,2-^{3}H-(*N*)]-hexadecyl ether; HPTS, 1-hydroxypyrene-3,6,8-trisulfonic acid; HSPC, hydrogenated soy phosphatidylcholine; mAb, monoclonal antibody; IC_{50}, inhibitory concentration for 50% cell growth; IgG, immunoglobulin; MM, multiple myeloma; MTT, 3-[4,5-dimethylthiazol-2-yl]-2,5,-diphenyltetrazolium bromide; NAM, *N*-acetylmethionine; NBD-PE, 12-[*N*-(nitrobenz-2-oxa-1,3-diazol-4-yl)amino]dodecanoyl phosphatidylethanolamine; NSIL, isotype-matched sterically stabilized immunoliposomes; PBMC, peripheral blood mononuclear cells; PBS, phosphate-buffered saline; PC40, partially hydrogenated egg phosphatidylcholine; PEG, poly(ethyleneglycol); PhE, phycoerythrin; SL, sterically stabilized liposomes; SIL, sterically stabilized immunoliposomes

* Corresponding author. Fax: +1-780-492-8078; E-mail: terry.allen@ualberta.ca

[1] Present address: Department of Advanced Therapeutics, B.C. Cancer Agency, Vancouver, BC, Canada V5Z 4E6.

0005-2736/00/$ – see front matter
PII: S0005-2736(00)00203-0

1. Introduction

Multiple myeloma (MM) is a malignancy of the immune system; it is identified clinically by the presence of terminally differentiated neoplastic plasma cells in the bone marrow [1]. Although most patients with MM initially respond to conventional chemotherapy, nearly all relapse within 1–2 years. Both aggressive combination chemotherapy and high dose chemotherapy followed by a bone marrow transplant increase the relapse-free interval; however, in most cases the disease eventually recurs and is refractory to further treatment [1–3].

Recent reports on MM have described a circulating population of monoclonal $CD19^+$ B cells [4–6] that exhibit extensive DNA aneuploidy [7] and display traits consistent with the invasive progenitors of plasma cells [8–11]. These monoclonal cells also express a functional p-glycoprotein plasma membrane transporter (P-gp) [12,13] that has been implicated in drug resistance and is correlated with chemotherapeutic failure [14,15]. Current therapies for MM have focussed on eradicating the malignant plasma cells in bone marrow, but such therapies have been largely unsuccessful in preventing relapse [1,3]. It has been suggested that, in MM, chemotherapy does not eliminate the malignant B cells in the blood and that relapse occurs because these cells repopulate the bone marrow [4,6–8,14].

The CD19 receptors present on the circulating monoclonal B cells seen in MM are known to be internalizing; these receptors have been implicated in a number of signalling functions [16–19]. Further, the binding of monoclonal antibody (mAb) to these receptors has been shown to trigger a cascade of intracellular messages that commit cells to differentiate and/or undergo cell-cycle arrest or apoptosis [16,20]. Thus, a possible approach to the eradication of malignant B cells in the blood of MM patients may involve the use of immunoliposomal anticancer drugs targeted against the CD19 antigen, or other internalizing antigens, on B cells. This receptor has already been a target for a number of antibody-based therapies; pre-clinical and clinical trials are currently underway to determine the effect of several treatment variations (free mAb, radiolabelled mAbs or immunotoxins [17,21–26]) on a variety of B cell cancers. It is possible that coupling of mAbs, such as anti-CD19, to long-circulating liposomal drugs will have advantages beyond those realized by specifically targeting receptors on the malignant cells. For instance, higher drug to antibody ratios can be achieved by using liposomal drug delivery systems; in addition, attaching the mAb at the terminus of poly(ethyleneglycol) (PEG) results in longer circulation half-lives for the targeted liposomes, which may, in turn, increase the binding and uptake of liposomal drugs by circulating malignant cells [27–29].

Immunoliposomal therapy has been shown to be effective in models of solid tumors in animals [29–31] and in the treatment of a murine xenograft model of human B cell lymphoma [32]; however, its applicability to treatment of MM remains uncharacterized. We hypothesize that in MM, treatment with immunoliposomes will selectively eradicate the circulating malignant $CD19^+$ B cell population while causing minimal toxicities to normal tissues (including T cells, thereby preserving the immune responses mediated by them). Besides eliminating these cells (which, as previously mentioned, may prevent relapse and improve patient survival by keeping these cells from reaching bone marrow and extra-skeletal tissues), immunoliposomal therapy may initiate endocytosis triggered by the internalizing CD19 receptor, thus bypassing membrane drug transporter(s) and allowing delivery of high levels of the cytotoxic agent to otherwise resistant cells [13,14].

To test our hypothesis, we evaluated the targeting and cytotoxicity of anti-CD19 immunoliposomal doxorubicin (DXR) to both monoclonal B cell lymphocytes from the blood of patients with MM and to a human MM cell line (ARH77). Two formulations of DXR-sterically stabilized immunoliposomes (DXR-SIL) (prepared with phospholipids (PLs) having different phase transition temperatures) were compared with respect to their binding, intracellular trafficking and cytotoxicity to $CD19^+$ myeloma cells.

2. Materials and methods

2.1. Chemicals

PEG, molecular weight 2000, covalently linked to distearoyl phosphatidylethanolamine (PEG_{2000}-DSPE), hydrazide-derivatized PEG-DSPE (Hz-

PEG-DSPE), hydrogenated soy phosphatidylcholine (HSPC) and partially hydrogenated egg phosphatidylcholine with an iodine number 40 (PC40) were generous gifts from SEQUUS Pharmaceuticals (Menlo Park, CA, USA) [33–35]. Cholesterol (CHOL) and 12-[*N*-(nitrobenz-2-oxa-1,3-diazol-4-yl)amino]dodecanoyl phosphatidylethanolamine (NBD-PE) were purchased from Avanti Polar Lipids (Alabaster, AL, USA). 1-Hydroxypyrene-3,6,8-trisulfonic acid (HPTS) was obtained from Molecular Probes (Eugene, OR, USA). Sephadex G50, Sepharose CL-4B and Ficoll-Paque were obtained from Amersham Pharmacia Biotech (Uppsala, Sweden). *N*-Acetyl-methionine (NAM), sodium periodate, 4,6-diamidino-2-phenylindole (DAPI) and 3-[4,5-dimethylthiazol-2-yl]-2,5-diphenyltetrazolium bromide (MTT) were purchased from Sigma (St. Louis, MO, USA). DXR (adriamycin RDF) was obtained from Adria Laboratories (Mississauga, Ont., Canada). RPMI 1640 media without phenol red, penicillin-streptomycin and fetal bovine serum (FBS) were purchased from Gibco BRL (Burlington, Ont., Canada). Cholesteryl-[1,2-^{3}H-(*N*)]-hexadecyl ether ([^{3}H]-CHE), 1.48–2.22 TBq/mmol, was purchased from New England Nuclear (Mississauga, Ont., Canada). Scintillation fluor/aqueous counting scintillant (ACS) was purchased from Amersham Canada (Oakville, Ont., Canada). Nucleopore polycarbonate filtration membranes (pore sizes: 0.4, 0.2, 0.1 and 0.08 μm) were obtained from Corning Costar (Kennebunk, ME, USA). All other chemicals, which came from various sources, were of analytical grade purity.

2.2. Antibodies, human cells and cell lines

Murine mAb anti-CD19 (IgG2a, immunoglobulin 2a) (from FMC63 murine CD19 hybridoma) and isotype-matched control IgG2a (IAG.11) were obtained from Dr. H. Zola (Child Health Research Institute, Adelaide, Australia) [18,36]. The MAbs anti-CD19 (IgG1), anti-CD22 (IgG1) and the isotype-matched control (IgG1) were a generous gift from Dr. E. Vitetta (University of Texas Southwestern Medical Centre, Dallas, TX, USA). Anti-CD45-phycoerythrin (anti-CD45-PhE) was mAb 17G10 from Dr. J. Wilkins (University of Manitoba, Winnipeg, Man., Canada). Mouse monoclonal antibodies specific for human leukocyte differentiation antigens CD4, CD8 and CD20 were either prepared in one of our laboratories or purchased from Coulter (Hialeah, FL, USA) or Becton Dickinson (San Jose, CA, USA). The concentrations of all laboratory mAbs were determined by using spectrophotometry ($\lambda = 280$ nm) and BioRad protein assays; their purity was assessed by sodium dodecyl sulfate–polyacrylamide gel electrophoresis. The reactivities of mAb were checked prior to use by indirect immunofluorescence using fluorescein isothiocyanate (FITC)-labelled goat anti-mouse Ab and flow cytometry (Becton Dickinson, San Jose, CA, USA) against appropriate cell lines, followed by comparison with appropriate FITC or PhE-conjugated isotype-matched controls.

Human peripheral blood mononuclear cells (PBMC) from MM patients were obtained after informed consent. Patients in this study were either newly diagnosed with the disease or were already undergoing chemotherapy. PBMC were isolated via Ficoll-Paque density gradient centrifugation (Pharmacia). Briefly, blood obtained from MM patients was diluted 1:1 with phosphate-buffered saline (PBS) and carefully layered on 20 ml Ficoll-Paque in a 50 ml polypropylene tube. The tubes were centrifuged for 25 min at 1800 rpm. After centrifugation and prior to experimental use, PBMC were collected from the interface, washed with PBS and re-suspended at a density of 1×10^7 cells/ml in RPMI 1640 media containing 10% FBS. Their viability was then assessed by staining with eosin, then using a haemocytometer to count the percentage of dead (i.e. stained) cells.

The human MM cell line ARH77 (ATCC CRL1621) was obtained from the American Type Culture Collection (Rockville, MD, USA). ARH77 cells were grown as suspension cultures in RPMI 1640 with no phenol red, supplemented with 10% heat-inactivated FBS and 1% penicillin-streptomycin (10 000 unit/ml penicillin G and 10 000 μg/ml streptomycin sulfate). Cells were maintained at 37°C in a 90% humidified incubator containing 5% CO_2. All experiments were performed on mycoplasma-free cell lines. For in vitro experiments, only cells in the exponential phase of growth were used.

2.3. Immunophenotyping of MM cells

Flow cytometry was used to phenotype the human

MM cell line (ARH77) and peripheral blood mononuclear cells (PBMC) from MM patients with antibodies against lymphocyte differentiation antigens (see Table 1). These antibodies were either purified mAbs or were conjugated to FITC or PhE. Briefly, ARH77 cells (1×10^6 cells) were incubated in darkness with 10 μg mAb/10^6 ARH cells at 4°C for 30 min in a total volume adjusted to 50 μl with PBS. After incubation, cells were washed three times with immunofluorescence buffer (IF buffer: PBS-containing 1% FBS and 0.1% sodium azide) and analyzed by flow cytometry. For indirect staining, subsequent to addition of primary Ab and washing, cells were incubated with 50 μl of 1:20 dilution of goat anti-mouse-FITC IgG (Sigma) in PBS at 4°C for 30 min. In some cases, cells were fixed with 1% formalin in PBS. Cell-associated fluorescence was analyzed on Becton Dickinson FACScan using LYSIS II software (Becton Dickinson, San Jose, CA, USA). FITC and PhE fluorescent markers were excited with an argon laser (488 nm) and the emitted fluorescence was detected through 530 (FITC) or 560 nm (PhE) band pass filters, respectively.

Table 1
Immunophenotyping of ARH cells or PBMC from MM patients using flow cytometry

Leukocyte differentiation antigens	Relative expression on cells[a]	
	ARH cells	PBMC
CD4 (T cell)	−	++1/2
CD8 (T cell)	−	+++
CD19	+1/2	++1/2
CD20	+++	+++
CD45	+++	++
IgG1(control)	−	−
IgG2a (control)	−	−

The human MM cell line ARH77, or PBMC from MM patients, were incubated with appropriate mAbs (10 μg mAb/10^6 cells) at 4°C for 30 min. Cell surface markers were evaluated by immunostaining with specific Abs, by either direct or indirect immunofluorescent staining methods (see Section 2). Cells were washed with IF buffer and cell-associated fluorescence was analyzed on a Becton Dickinson flow cytometer.

[a]The reactivities of mAbs with cells were scored relative to their mean fluorescence intensity (MFI) of staining using flow cytometry: ++++ MFI 10^4 (very high); +++ MFI 10^3 (high); ++ MFI 10^2 (moderate); + MFI 10^1 (low); +/−;MFI $10^{0.5-1}$ (very low); − MFI $<10^{0.5}$ (negative). Unstained control cells were set at $<10^{0.5}$ MFI.

2.4. Preparation of liposomes

Liposomes were composed of either HSPC:CHOL:mPEG$_{2000}$-DSPE (2:1:0.1 molar ratio) or PC40:CHOL:Hz-PEG$_{2000}$-DSPE (2:1:0.1 molar ratio). In some preparations, [^{3}H]CHE was added as a non-exchanged, non-metabolized lipid tracer [37,38]. Fluorescent-labelled liposomes were prepared by incorporating NBD-PE (1 mol%) into the lipid mixture. Dried lipid films were hydrated using a solution of 25 mM HEPES (pH 7.4) and 140 mM NaCl or 155 mM ammonium sulfate pH 5.5 (for DXR loading), then sequentially extruded (Lipex Biomembranes Extruder, Vancouver, BC, Canada) through polycarbonate filters of varying pore sizes (0.08–0.4 μm) to produce vesicles 95–110 nm in diameter [39]. Liposome size was characterized on a Brookhaven BI90 particle sizer (Brookhaven Instruments, Holtsville, NY, USA). PL concentrations were determined by using either the specific activity counts of [^{3}H]CHE tracer or the Bartlett colorimetric assay [40]. The number of liposomes in the liposome dispersion was estimated at 7.7×10^{12} liposomes/μmol PL [32,41].

DXR was remote-loaded via an ammonium sulfate gradient method previously described [32,42]. Liposome-encapsulated DXR was separated from free DXR on a Sephadex G-50 column equilibrated with 123 mM sodium citrate (pH 5.5). The concentration of the liposome-entrapped DXR was 150 μg DXR/μmol PL (0.26 μmol DXR/μmol PL, as determined by spectrophotometry ($\lambda=480$ nm in methanol).

By using a previously described hydrazide coupling method [32,43], antibodies were coupled to the terminus of pre-formed liposomes that contained the coupling lipid Hz-PEG-DSPE. From the specific activity of the ^{125}I-anti-CD19 label incorporated during coupling, we calculated the concentration of anti-CD19 on liposomes to be 50 μg anti-CD19/μmol PL. On the basis of a concentration of 7.7×10^{12} liposomes/μmol PL, we calculated that there were approximately 25 antibodies/liposome [32].

2.5. Cell uptake experiments

ARH77 cells were plated in 48-well tissue culture plates at 1×10^6 cells/100 μl RPMI 1640 supple-

mented with 10% FBS. Various formulations of ^{3}H-CHE-labelled liposomes, with or without coupled anti-CD19, were added to each well (200 μl total volume, 50–1600 nmol/ml) and maintained at 37°C with 90% humidity and 5% CO_2. After 1 h incubation, the cells were washed three times with cold PBS (pH 7.4) and cell-associated liposomes were determined from the initial specific activity of the ^{3}H-CHE-liposomes.

In some experiments, the association of cells with immunoliposomes labelled with 1 mol% of the fluorescent lipid marker NBD-PE was determined by flow cytometry. Various formulations of NBD-PE-labelled liposomes (400 nmol PL/ml) were incubated (for 1 or 24 h at 37°C) with 1×10^{6} ARH77 cells. In competition experiments, targeted NBD-SIL[anti-CD19] liposomes were incubated with a 30-fold excess of free anti-CD19 (6.4×10^{-4} μmol anti-CD19). Cells were washed three times with IF buffer and fixed in 1% formalin prior to analysis on the flow cytometer. Cell debris was excluded by appropriate gating on 'forward' versus 'side angle' scatter profiles. Data were recorded from 5000–20 000 events and later analyzed using the LYSIS II software program (Becton Dickinson, San Jose, CA, USA). For two-color immunofluorescence experiments with PBMC from MM patients, cells were labelled with, in addition to fluorescent liposomes, either anti-CD20-PhE (B cell marker) or a combination of anti-CD4-PhE and anti-CD8-PhE (T cell markers), which allowed us to identify the individual lymphocyte populations.

To determine the association of DXR with ARH77 cells using flow cytometry, cells were incubated with either free DXR or various liposomal DXR formulations at concentrations of drug ranging from 0.1 to 100 μg/ml for 1, 4 or 24 h at 37°C. Cells were then washed with cold IF buffer and immediately run on a Becton Dickinson FACScan (Becton Dickinson, San Jose, CA, USA). Cell-associated DXR was excited with an argon laser (488 nm) and the fluorescence was detected at 560 nm. Files were collected of 20 000 ungated events and analyzed with the LYSIS II software program.

The internalization of liposomes by ARH77 cells was studied using the encapsulated pH-sensitive fluorescent probe HPTS (pyranine); this technique has been described elsewhere [44,45]. Cells (1×10^{6}/well) were incubated, at 37°C for either 1 or 24 h, with various formulations of HPTS-liposomes at a final PL concentration of 400 nmol/ml. They were then washed three times with PBS; the cell-associated fluorescence spectrum was then determined by scanning the excitation spectra from 320 to 500 nm, with the emission wavelength fixed at 510 nm. From the excitation spectra of the HPTS molecules, the pH of the liposomal environment upon interaction with ARH77 cells was determined from a previously prepared standard curve of the free HPTS ranging from pH 5 to 9.

The intracellular distribution of liposomes was determined using confocal laser scanning microscopy. PBMC from MM patients (1×10^{6} cells/well) were incubated with either free DXR or liposomal formulations of DXR (20 μg/ml in a total volume of 500 μl media) for 1 h at 37°C. After incubation, cells were washed with cold PBS and stained for 30 min with anti-CD19-FITC. Cells were allowed to adhere onto poly-L-lysine-coated slides prior to mounting with PermaFluor (Lipshaw Immunon, Pittsburgh, PA, USA). Cells were visualized on a Leitz Aristoplan Fluorescence Microscope illuminated by a 100 W HBO mercury burner for direct observation and an argon–krypton laser with major emissions at 488, 568 and 647 nm for scanning observations. Cells were optically sectioned over a random field of cells. Images (512×512 pixel) were stored on optical disks for further analyses using Leica Lasertechnick (Heidelberg, Germany) software. All instrumental parameters pertaining to fluorescence illumination, detection and image analyses were held constant as follows: 100/1.32 oil-immersion objective lens, pinhole 100, off-sets −29/−30, KP590 short-pass excitation filter, neutral beam-splitter, barrier long-pass filter OG 590, and a photomultiplier gain of 790 V.

2.6. Cytotoxicity experiments

The MTT proliferation assay was used to compare the cytotoxicities of various liposomal formulations to CD19+ARH77 cells [46]. These formulations included free DXR, DXR-HSPC-SL, DXR-HSPC-SIL[anti-CD19] and DXR-HSPC-NSIL[IgG2a] with or without free mAb anti-CD19 or isotype-matched control IgG2a. In some experiments, PC40 was substituted for HSPC. The IC_{50} (inhibitory concentra-

tion for 50% cell growth) was determined as described in a previous publication [32].

The cytotoxicity of DXR or liposomal DXR to the B lymphocyte populations in PBMC samples from myeloma patients was evaluated using DAPI binding to quantify apoptotic cells [47,48]. Treatment groups were assigned to each patient sample, depending upon the number of PBMC isolated from individual patients. PBMC (2×10^6 cells/well) were incubated with either DXR or different formulations of liposomal DXR for 24 h at 37°C. After incubation, cells were washed, re-plated and incubated for an additional 48 h at 37°C in RPMI 1640 media plus 10% FBS. At the end of the assay, cell viability was assessed using eosin dye exclusion. Myeloma PBMC were stained with the appropriate mAbs for detecting B (anti-CD19-FITC) or T (anti-CD4,8-PhE) cells, as well as with DAPI to detect DNA content. DAPI staining was done on ethanol-permeabilized (70% ethanol at 4°C) and RNase-treated cells at a final DAPI concentration of 1.5 μg/ml. Chicken red blood cells (Crbc), which have one-third the cellular DNA content of human red blood cells, were used as an internal standard. The positions of the B and T cell diploid peaks were set relative to the Crbc peak. Samples were immediately run on the Elite flow cytometer (Coulter, Hialeah, FL, USA), with both FITC and PhE excited at 488 nm by the argon laser and simultaneous UV excitation of DAPI at 353 nm by the water-cooled laser. Files of 10 000–40 000 events were collected and these were ungated to prevent the exclusion of any drug-induced apoptotic cells. Files were analyzed by listmode using the ELITE software (Coulter). Electronic gates were set for B cells or T cells to evaluate individual DAPI profiles against appropriate FITC or PhE isotype-matched mAb controls. B cells consisted of all CD19-positive, CD4,8-negative cells. Cell doublets were excluded during analyses by appropriate gating on DAPI intensity versus DAPI peak. The histogram profiles of DAPI staining of T cells were first analyzed to identify the position of the diploid peak (2*N* number of chromosomes) relative to the Crbc internal standard. In order to include untreated cells within this marker, the diploid peak marker was set at twice the standard deviation (i.e. 95% confidence interval). Relative to this diploid peak (2*N*), appropriate statistical markers were selected to identify cells having a hypodiploid DNA content (at least 2S.D. lower than that of autologous diploid T cells), which is indicative of apoptosis.

2.7. Statistical analyses

All linear regression analyses were performed using Quattro Pro 4.0 (Borland, Scotts Valley, CA, USA). Unless otherwise stated, the two-tailed Student's *t*-test (INSTAT, GraphPAD software, version 1.11a) was used to measure statistical significance, assuming equal variances with 95% confidence intervals. Using one-way analysis of variance, multiple comparisons of various groups in cytotoxic assays were evaluated, again on INSTAT. Post-tests to compare the various treatment means were performed using Bonferroni's tests. Data were considered statistically significant at $P<0.05$. Data are reported as mean ± standard deviation (S.D.).

3. Results

3.1. Cell immunophenotyping

The expression of selected leukocyte differentiation antigens on ARH77 and BPBMC cells (containing both B and T cells) from MM patients was compared with that of controls stained with their appropriate isotype-matched IgG1 or IgG2a antibodies conjugated to FITC or PhE (Table 1). Anti-CD19 bound to ARH77 cells and to PBMC cells from MM patients, presumably to a population of B cells (Table 1). Antibodies to CD4 and CD8 did not bind to B cells, but did bind to PBMC, presumably to the T cell population in patients' blood. B cell mAbs did not cross-react with the T cell lymphoma cell line H9 (not shown). Using flow cytometry after staining with anti CD19-FITC, the number of CD19 receptors on ARH77 cells was estimated by comparing the MFI of ARH77 cells with that of the human B lymphoma cell line (Namalwa), which expresses approximately 40 000 CD19 receptors per cell. [18,49,50]. From the binding curves of free anti-CD19-FITC to ARH77 cells (at saturation binding), the relative density of CD19 receptors on ARH77 cells was estimated at approximately 3000 sites per cell (not shown).

3.2. Cell uptake experiments

Binding experiments were conducted using ^{3}H[CHE]-labelled liposomes (Fig. 1). SIL[anti-CD19] showed a two- to three-fold higher binding to ARH77 cells than to either non-targeted SL (sterically stabilized liposomes) or isotype-matched control liposomes NSIL[IgG2a] (Fig. 1). At maximum binding there were approximately 6.9×10^{-4} or 2.1×10^{-4} μmol PL binding sites/10^{6} cells for SIL[anti-CD19] and SL, respectively. The dissociation constant K_D for the SIL[anti-CD19] was estimated at 220 μM, which was two-fold lower that for SL.

Using flow cytometry, similar experiments were performed using 1-h incubations of fluorescent NBD-PE-labelled HSPC-CHOL liposomes (Fig. 2). ARH77 cells showed greater binding of free anti-CD19-FITC than did irrelevant IgG2a-FITC or untreated cells (Fig. 2a). Increased binding was not observed for either SL or NSIL[IgG2a] to ARH77 cells (Fig. 2b), but SIL[anti-CD19] binding was twice that of non-targeted liposomes (Fig. 2b versus c). Competition with excess free anti-CD19 was able to inhibit the binding of SIL[anti-CD19] with ARH77 cells, indicating binding specificity of the immunoliposomes (Fig. 2c). Similar two-fold increases in binding were observed at 1 h for a more fluid formulation composed of PC40:CHOL (not shown). With 24-h incubations, non-specific association of non-targeted liposomes (SL) to ARH77 cells increased approximately five-fold over that of the 1-h incubations, but the binding of immunoliposomes was still two-fold higher than the binding of non-targeted liposomes (not shown).

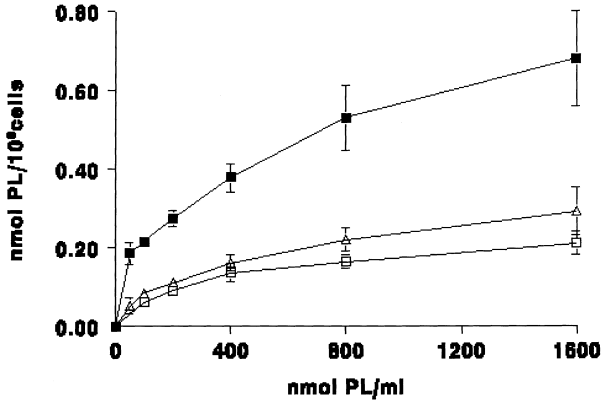

Fig. 1. Binding of [^{3}H]CHE-labelled liposomes by ARH77 cells as a function of liposome concentration. Liposomes 104 nm in diameter were composed of either HSPC:CHOL:PEG_{2000}-DSPE, 2:1:0.1 ± mAb anti-CD19 or isotype-matched control mAb IgG2a attached via a hydrazone bond at the PEG terminus, at approximately 50 μg mAb/μmol PL. SL (□), SIL[anti-CD19] (■) or NSIL[IgG2a] (△) were incubated with 10^{6} ARH77 cells for 1 h at 37°C. Data are expressed as nmol PL ± S.D. per 10^{6} cells ($n=3$).

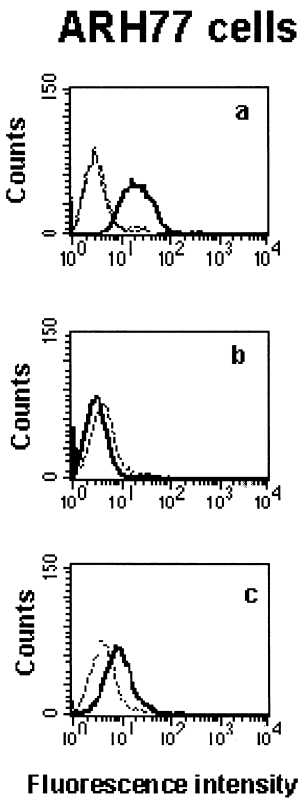

Fig. 2. In vitro binding of fluorescent NBD-labelled liposomes to ARH77 cells using flow cytometry. NBD-labelled liposomes 105 nm in diameter (0.1 mol%) were composed of either HSPC:CHOL:Hz-PEG-2000-DSPE (2:1:0.1 molar ratio) ± mAb anti-CD19 or isotype-matched control IgG2a. ARH77 cells were incubated with various formulations of liposomes (400 nmol PL/ml) for 1 or 24 h at 37°C. Excitation was at 480 nm (argon laser) and emission at 510 nm. Histogram overlays illustrate: (a) unstained cells (dotted line) or cells treated with either irrelevant antibody IgG2a-FITC (dashed line) or anti-CD19-FITC (bold line); (b) SL (dotted line) or NSIL-[IgG2a] (bold line) at 1 h; (c) free anti-CD19+SIL[anti-CD19] (dashed line) and SIL[anti-CD19] (bold line) at 1 h.

ARH77 cells (1×10^{6} cells/well) were incubated (for 1 and 24 h at 37°C) with either free DXR or liposomal DXR at a DXR concentration of 20 μg DXR/ml. Relative cell-associated DXR was analyzed using flow cytometry (Fig. 3). Free DXR rapidly

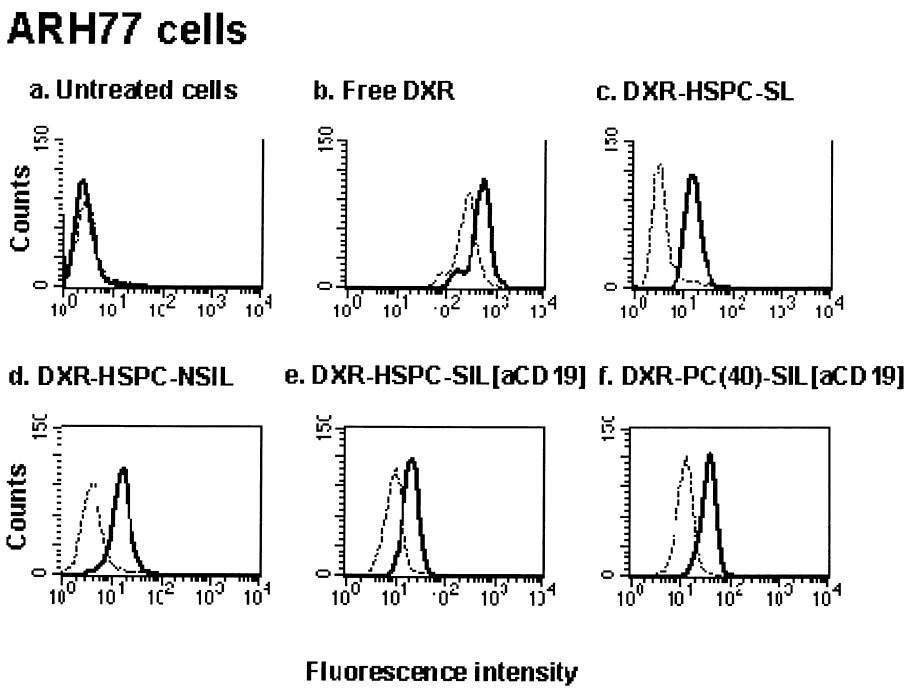

Fig. 3. Flow cytometric analyses of the association of free DXR and liposomal DXR with ARH77 cells. ARH77 cells (1×10^6 cells/well) were incubated with either free DXR or various formulations of liposomes 108 nm in diameter at a final DXR concentration of 20 μg/ml for either 1 h (dotted line) or 24 h (bold line) at 37°C. Cells were washed and cell-associated DXR was evaluated using flow cytometry. Histogram overlays illustrate: (a) untreated cells; (b) free DXR; (c) DXR-SL (no mAb); (d) DXR-NSIL[IgG2a]; (e) DXR-HSPC-SIL[anti-CD19]; and (f) DXR-PC40-SIL[anti-CD19].

accumulated in ARH77 cells within 1 h at 37°C (Fig. 3b). The two targeted formulations (Fig. 3e,f) had three-fold higher DXR levels at 1 h than the non-targeted formulations (Fig. 3c,d). The cellular DXR levels for the two targeted formulations were 5–8-fold lower than that seen for free DXR (Fig. 3e,f, versus b). At 24 h, DXR-HSPC-SIL[anti-CD19] had DXR levels twice that of the non-targeted formulations (Fig. 3e versus c,d). As expected, higher cellular DXR levels were seen at 24 h for the leakier PC40-containing targeted formulation relative to the relatively non-leaky HSPC targeted formulation (1.5-fold increase, Fig. 3e versus f).

To determine whether receptor-mediated internalization of immunoliposomes is triggered by binding of SIL[anti-CD19] liposomes to ARH77 cells, we used a previously described spectrofluorimetric assay [44,45]. Incubation of ARH77 cells at 37°C for 1 h with HSPC-SIL[anti-CD19] or PC40-SIL[anti-CD19], both of which contained entrapped HPTS, was associated with a drop in pH from pH 7.3 to pH 6.5–6.6 ($P<0.01$) (Fig. 4). A further drop in pH occurred after 24-h incubations (Fig. 4C). Both formulations of SIL[anti-CD19] appeared to internalize at similar rates and to similar extents (Fig. 4) ($P>0.05$). No pH change was observed when SIL-[anti-CD19] were incubated with the control $CD19^-$ T cell line H9 (not shown). The internalization of liposomal HPTS into ARH77 cells was inhibited at 4°C or by 0.1% sodium azide (Fig. 4A and D), suggesting a metabolic requirement for the acidification of liposomal HPTS. No pH drop was observed for either the non-targeted SL or the isotype-matched control liposomes (NSIL[IgG2a]) ($P>0.05$), a finding consistent with non-specific absorption of liposomes at the cell surface (Fig. 4).

3.3. Cytotoxicity experiments

As shown in Table 2, after 1 h incubation DXR-HSPC-SIL[anti-CD19] or DXR-PC40-SIL[anti-CD19] were more cytotoxic to ARH77 cells than were their non-targeted counterparts, DXR-HSPC-SL ($P<0.01$), DXR-PC40-SL ($P<0.01$) or DXR-

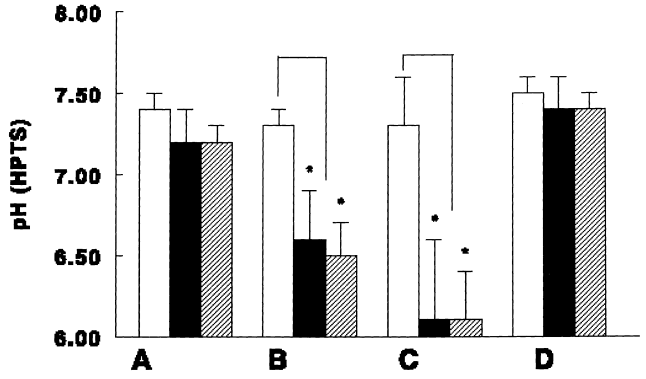

Fig. 4. Internalization of liposomal HPTS by ARH77 cells. Liposomes 109 nm in diameter were composed of HSPC:CHOL:Hz-PEG$_{2000}$-DSPE:mAb anti-CD19 or PC40:CHOL:Hz-PEG$_{2000}$-DSPE: mAb anti-CD19, both at a 2:1:0.1:0.002 molar ratio (50 μg anti-CD19/μmol PL) and containing encapsulated HPTS. ARH77 cells were exposed to either HPTS-SL (empty bars), HPTS-HSPC-SIL[anti-CD19] (solid bars) or HPTS-PC40-SIL[anti-CD19] (hatched bars) under the following treatment conditions: (A) 1 h, 4°C; (B) 1 h, 37°C; (C) 24 h, 37°C; or (D) sodium azide-treated ARH77 for 1 h at 37°C. The pH environment of the liposomes inside cells was determined from the ratio of the excitation peaks, 403/413 to 450/413 nm ($n=3$). *Student's t-test, $P<0.01$.

HSPC-NSIL[IgG2a] ($P<0.001$). The IC$_{50}$ of the leakier formulation DXR-PC40-SIL[anti-CD19], which was lower than that of DXR-HSPC-SIL[anti-CD19] ($P<0.001$), was equivalent to the cytotoxicity of free DXR ($P>0.05$) after 1 h incubation at 37°C (Table 2). At 24 h, the IC$_{50}$s of all DXR-formulations were reduced ($P<0.01$) (Table 2). At 24 h, DXR-PC40-SIL[anti-CD19] were more cytotoxic than free DXR ($P<0.001$), DXR-HSPC-SIL[anti-CD19] ($P<0.001$) or non-targeted DXR-PC40-SL ($P<0.05$). HSPC-SIL[anti-CD19] were 17–27 times more cytotoxic than either DXR-HSPC-SL or DXR-HSPC-NSIL[IgG2a] at 1 h and 8–11 times more cytotoxic at 24 h (Table 2), suggesting that, at later times, non-specific association of liposomes and leakage may contribute to the cytotoxicity of non-targeted liposomes. MAb contributed little to the cytotoxicity; free anti-CD19 had an IC$_{50}$ of greater than 1.28 μM (Table 2). In comparison, at the IC$_{50}$ for DXR-SIL[anti-CD19] of 9.97 μM, the amount of coupled anti-CD19 was equivalent to a mAb concentration of 10 nM. Empty SIL[anti-CD19] (no drug), at comparable antibody densities, showed low cytotoxicity to ARH77 cells (Table 2).

To determine whether the free anti-CD19 sensitizes cells to DXR, we co-incubated cells with 3.2×10^{-7}

Table 2
Cytotoxicity of various liposomal formulations, free drug or free anti-CD19

Treatment[a]	IC$_{50}$, 1 h	IC$_{50}$, 24 h
Drug-free SIL[anti-CD19] (PL)	>1500	580
Free DXR (DXR)	1.28±0.16	0.47±0.03
DXR-HSPC-SL (DXR)	265.8±32.0	10.4±0.6
DXR-HSPC-NSIL[IgG2a] (DXR)	165.8±17.2	7.9±2.2
DXR-HSPC-SIL[anti-CD19] (DXR)	9.97±2.3	0.98±0.02
DXR-PC40-SL (DXR)	2.75±0.30	0.33±0.06
DXR-PC40-SIL[anti-CD19] (DXR)	1.06±0.29	0.16±0.05
Free anti-CD19 (mAb)	>1.28	>1.28
Free IgG2a isotype match (mAb)	>1.28	>1.28
Anti-CD19+free DXR (DXR)	1.06±0.40	0.09±0.02
Anti-CD19+DXR-HSPC-SL (DXR)	245.0±59.8	75.6±37.8
Anti-CD19+DXR-HSPC-SIL[anti-CD19] (DXR)	235.2±32.4	23.7±2.7
IC$_{50}$ ratio, DXR-HSPC-SL:DXR-HSPC-SIL[anti-CD19]	26.7:1	10.6:1
IC$_{50}$ ratio, DXR-PC40-SL:DXR-PC40-SIL[anti-CD19]	2.6:1	2.1:1
IC$_{50}$ ratio, anti-CD19+DXR-SL:anti-CD19+DXR-SIL[anti-CD19]	1.1:1	3.2:1

ARH77 cells (5×10^5/well) were incubated with various treatments for 1 or 24 h, after which cells were washed and placed in wells containing fresh media. At 48 h, MTT solution (25 μg/well) was added to each well and the plates were further incubated for 4 h at 37°C. The colored formazan product was dissolved using 100 μl of acid-isopropanol and the plates were read on a Titertek Multiskan Plus (Flow Laboratories, Mississauga, Ont., Canada) at dual wavelengths 570 and 650 nm. Means±S.D., $n=3$.
[a]Notation in brackets indicates whether the IC$_{50}$ is for DXR, PL or Ab.

μmol of free anti-CD19 in addition to either free DXR or liposomal DXR in order to saturate all CD19 sites on ARH77 cells (Table 2). Free anti-CD19 and non-specific IgG2a were not cytotoxic in the concentration range tested (Table 2). Comparing the IC_{50} after 1-h incubations, there was no difference between the cytotoxicities of either free DXR or free DXR combined with anti-CD19 ($P > 0.05$). The cytotoxicity of DXR-SL plus anti-CD19 was comparable to that of DXR-SL alone ($P > 0.05$) (Table 2). The combination of free anti-CD19 with DXR-SIL[anti-CD19] increased the IC_{50} of the liposomes by 24-fold ($P < 0.001$), similar to that of non-targeted DXR-SL ($P > 0.05$). This indicates that free anti-CD19 competitively inhibited the binding of DXR-SIL[anti-CD19] to ARH77 cells.

3.4. Interactions of immunoliposomes with PBMC from MM patients

We used two-color immunofluorescence and flow cytometry to determine whether SIL[anti-CD19] specifically bound B cells in heterogeneous populations of PBMC from MM patients (Fig. 5). NBD-PE-containing liposomes were incubated with PBMC; individual populations of B and T cells were identified by staining with anti-CD20-PhE or anti-CD4,8-PhE, respectively. B cells were stained with anti-CD20-PhE instead of anti-CD19-PhE because competition exists between binding of SIL[anti-CD19] and free anti-CD19 (see Fig. 2c). Fig. 5 shows a representative example of PBMC from one patient; it contained 9% B cells and 63% T cells. NBD-SL (Fig. 5A,B), or NBD-NSIL[IgG2a] (not shown), showed low binding to MM PBMC, with only 1% of B cells positive for both NBD-SL and anti-CD20 and only 2% of T cells labelled by both NBD-SL and anti-CD4,8 (Fig. 5A,B). In contrast, NBD-SIL[anti-CD19] selectively bound to B cells (7% of PBMC cells were dual-labelled, Fig. 5D, which corresponds to 78% specific labelling of B cells). In this patient's sample, 63% of the cells stained with CD4,8-PhE (Fig. 5C) but not NBD-SIL[anti-CD19] (Fig. 5C). A summary of the results for 10 patients is presented in Table 3. With the exception of one patient with 20% B cells, all patients had from 5–10% B cells in their PBMC. SIL[anti-CD19] specifically stained a larger proportion of B cells than T cells (72% versus

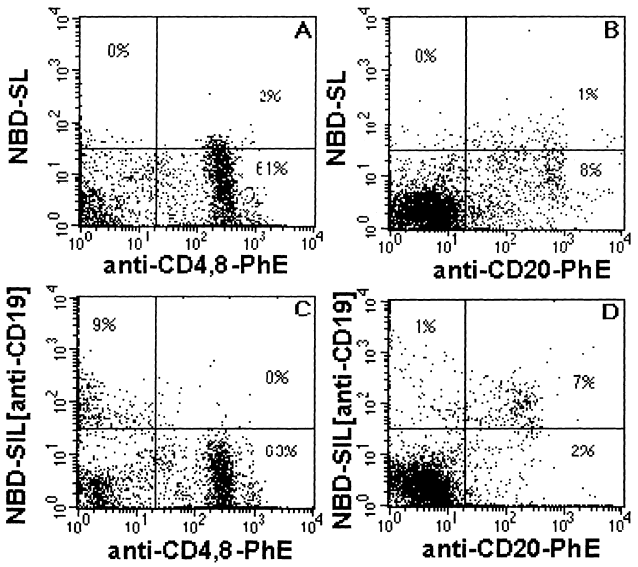

Fig. 5. Two-color flow cytometry of the binding of immunoliposomes by PBMC from a representative MM patient. Liposomes 107 nm in diameter were composed of HSPC:CHOL:PEG_{2000}-DSPE:NBD-PE (2:1:0.1:0.02 molar ratio) ± mAb anti-CD19. PBMC from a MM patient were incubated with either NBD-SIL[anti-CD19] or NBD-SL, then stained with either anti-CD20-PhE for B cells or anti-CD4,8-PhE for T cells. Dot plots illustrate the intensity of the two stains on cells treated with: (A) NBD-SL and anti-CD4,8-PhE; (B) NBD-SL and anti-CD20-PhE; (C) NBD-SIL[anti-CD19] and anti-CD4,8-PhE; or (D) NBD-SIL[anti-CD19] and anti-CD20-PhE.

5.3%, respectively, $P < 0.001$). Binding to B cells of SIL[anti-CD19] was significantly higher than binding of either SL (8.3%, $P < 0.001$) or NSIL[IgG2a] (6.7%, $P < 0.001$), but SL and NSIL[IgG2a] were not significantly different from each other.

Targeting and intracellular distribution of liposomal DXR in PBMC from MM patients were confirmed using confocal microscopy (Fig. 6). PBMC were incubated in vitro with liposomal DXR for 1 h at 37°C. Individual B and T cells were identified using anti-CD19-FITC for B cells and anti-CD4,8 to detect T cells. Free DXR rapidly stained the nuclei of both T cells (Fig. 6A) and B cells (Fig. 6B). Neither DXR-SL (Fig. 6C,D) nor DXR-NSIL[IgG2a] (not shown) showed an accumulation of DXR into either T (Fig. 6C) or B cells (Fig. 6D). The cell surface can be seen in the green channel, but there is little or no corresponding fluorescence for DXR in the red channel. DXR-SIL[anti-CD19] incubated with PBMC did not associate with T cells (Fig. 6E, green channel),

Table 3
Specific binding of liposomes to either B or T cells in heterogeneous mixtures of PBMC from MM patients

Liposome formulation	% $CD20^+$ B cells that bind liposomes	% $CD4,8^+$ T cells that bind liposomes
SL ($n=10$)	8.3 ± 5.3	2.6 ± 4.2
NSIL[IgG2a] ($n=3$)	6.7 ± 1.8	1.1 ± 0.3
SIL[anti-CD19] ($n=10$)	72.0 ± 20.5	5.3 ± 4.7

PBMC from MM patients were purified using Ficoll gradients. The percentage of B and T cells in PBMC isolated from each MM patient blood sample was determined by immunofluorescent staining with anti-CD19-FITC or anti-CD4,8-PhE, followed by two-color flow cytometric analysis. B and T lymphocytes in PBMC from MM patients ranged from 4–20 and 25–70%, respectively ($n=10$). PBMC were incubated with a liposome concentration of 400 nmol PL/ml. Liposome composition was HSPC:CHOL:Hz-PEG-DSPE:NBD-PE (2:1:0.1:0.02 molar ratio, 100–112 nm in diameter), with or without anti-CD19 or non-specific IgG2a. Specific labelling of individual cell populations by liposomes was determined by identification of cells with anti-CD20-PhE for B cells or anti-CD4,8-PhE for T cells (see Fig. 5). Means ± S.D.

but did associate with a population of non-T cells (Fig. 6E, red channel). Lack of co-localization of the green staining (T cell marker, anti-CD4,8-FITC) with the red staining (B cell marker, DXR-SIL[anti-CD19]) suggests that the T cell marker stained different cells than the immunoliposomes. When PBMC were stained with anti-CD19-FITC, DXR-SIL[anti-CD19] was found to co-localize with anti-CD19-FITC, confirming specificity for B cells (Fig. 6F, green versus red channels). Red punctate fluorescence within the cytoplasm of MM B cells suggests that internalization of DXR-SIL[anti-CD19] occurred (Fig. 6E,F, red channel).

The cytotoxicity of free DXR or liposomal DXR against PBMC from MM patients was evaluated by using two-color immunofluorescence and DAPI staining for DNA content. Crbc were used as an internal control to identify the position of diploid cells. Untreated PBMC from MM patients contained an average of 11 and 24% apoptotic T and B cells, respectively (Table 4). (Apoptotic cells are defined as those having a hypodiploid DNA content, i.e. showing more DAPI staining events in the hypodiploid (H) and apoptotic (A) regions, but fewer in the diploid and hyperdiploid regions [13].) A representative example from a single patient is shown in Fig. 7. T cells had a DNA content approximately three times that of the Crbc controls (as expected for diploid (D) cells), while B cells had increased DAPI staining in the hyperdiploid (4N) region (Fig. 7(1)). Fig. 7(2) shows that free DXR (5 μM) resulted in the death of both B and T cell populations, as is evidenced by increased staining in the H and A regions combined with decreased staining in the D and 4N regions (Fig. 7(2)). DXR-SL displayed minimal cytotoxicity to either B or T cells (Fig. 7(3)). In comparison, DXR-SIL[anti-CD19] were not cytotoxic to T cells, but did result in increased apoptosis to B cells (Fig. 7(4) versus (1)).

A summary of the results for 8 MM patient samples is presented in Table 4. In all patient samples, free DXR (5 μM) was equally cytotoxic to both B and T cell populations ($P > 0.05$). DXR-SIL[anti-CD19] was selectively apoptotic to B cells, with low cytotoxicity to T cells ($P < 0.001$); B cell cytotoxicity for the targeted liposomes was not significantly dif-

Table 4
Cytotoxicity of free DXR or various formulations of liposomal DXR to PBMC from MM patients

Treatment	Percent apoptotic cells	
	B cells	T cells
Untreated	24 ± 8	11 ± 6
Free DXR	85 ± 22	73 ± 19
DXR-SL	27 ± 11	13 ± 7
DXR-NSIL[IgG2a]	10 ± 3	5 ± 1.3
Empty SIL[anti-CD19]	21	18
DXR-SIL[anti-CD19]	62 ± 18	17 ± 9

Data represent single measurements or means of 2–4 replicates for an individual patient sample. PBMC from 8 MM patients were untreated or treated with free DXR or various liposomal DXR formulations (5 μM DXR). After incubation, cells were stained with anti-CD19-FITC, anti-CD4,8-PhE, and DAPI. Files were gated for either B ($CD19^+$) or T ($CD4,8^+$) cells; their DAPI profiles were plotted as DNA histograms (Fig. 7). The relative DNA content of cells was determined from the position of the diploid (2N) DNA peak of B and T cells, against a Crbc internal standard (Fig. 7A). Hypodiploid cells were defined as those having $<2N$ DNA (determined from their reduced DAPI binding). Means ± S.D.

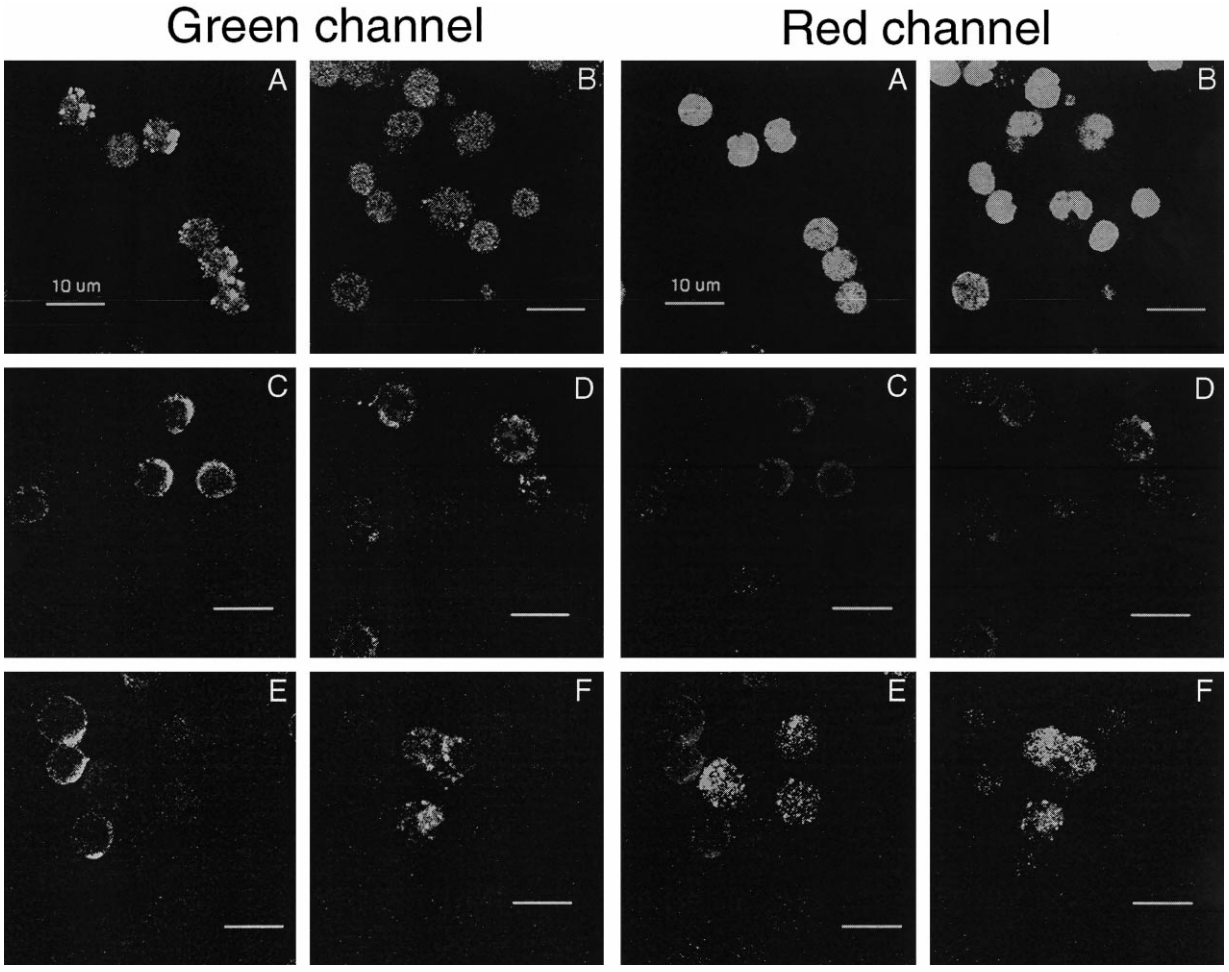

Fig. 6. Interaction of immunoliposomal DXR with PBMC from MM patients, as visualized using confocal microscopy. Liposomes were composed of HSPC:CHOL:Hz-PEG$_{2000}$-DSPE, 2:1:0.1 molar ratio (108 nm in diameter) ± mAb anti-CD19 or irrelevant mAb IgG2a and contained encapsulated DXR. PBMC from MM patients (2×10^6 cells) were incubated with either free DXR or various liposomal formulations of DXR at 20 μg DXR/ml for 1 h at 37°C. After incubation with liposomes, cells were washed and stained with anti-CD19-FITC or anti-CD4,8-FITC. Green channel, antibody (FITC) fluorescence; red channel, DXR fluorescence. (A) Free DXR and anti-CD4,8-FITC; (B) free DXR and anti-CD19-FITC; (C) DXR-SL and anti-CD4,8-FITC; (D) DXR-SL and anti-CD19-FITC; (E) DXR-SIL[anti-CD19] and anti-CD4,8-FITC; and (F) DXR-SIL[anti-CD19] and anti-CD19-FITC.

ferent from that of free DXR (Table 4). DXR-SIL[anti-CD19] treatment significantly increased the percentage of apoptotic B cells compared with DXR-SL, NSIL[IgG2a] or untreated controls ($P<0.001$, Table 4). Empty SIL[anti-CD19] were not cytotoxic at mAb and lipid doses were equivalent to those used for immunoliposomal DXR (Table 4).

4. Discussion

Our previous study on the use of immunoliposomal DXR to treat human B lymphoma suggested that this treatment may be applicable to other B cell malignancies, including MM [32]. In MM, large numbers of malignant B cells are present in blood and bone marrow [4,6,7]. This makes MM amenable to treatment with targeted immunoliposomal drugs, particularly sterically stabilized formulations that remain in the blood for prolonged times [51]. The work reported here demonstrates that DXR-SIL[anti-CD19] is selectively targeted to the human CD19$^+$ MM cell line ARH77 and to CD19$^+$ clonotypic B cells in PBMC from MM patients.

It has been previously shown that mAb anti-CD19 binds CD19 with a high affinity [18,36], whereas cou-

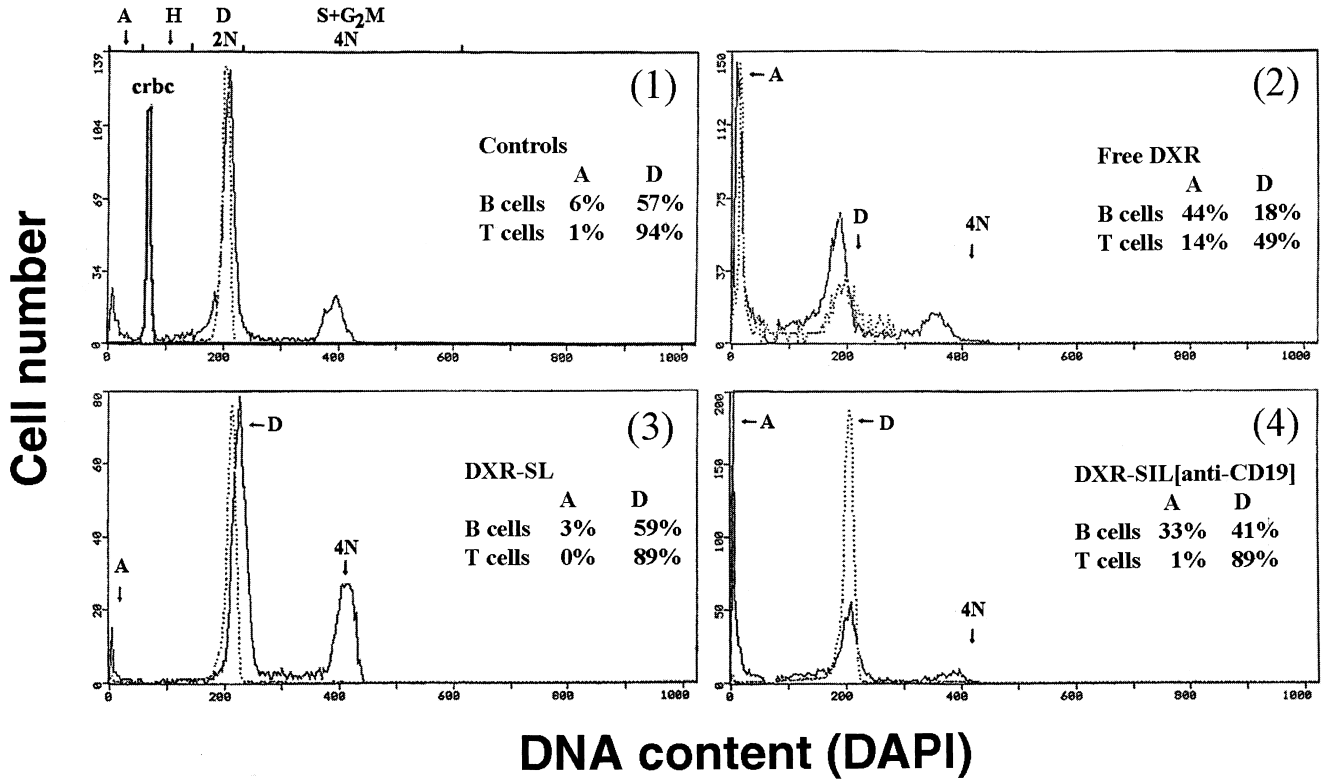

Fig. 7. In vitro cytotoxicity of free DXR and various liposomal DXR formulations from a MM patient PBMC (5 μM DXR concentration for all formulations). Gated populations of B (solid line) or T cells (dotted line) were selected by appropriate staining with either anti-CD19-FITC (B cells) or anti-CD4,8-PhE (T cells); each population was analyzed independently for its DAPI content. Histogram panels (1)–(4) illustrate DAPI profiles of PBMC from a single patient: (1) untreated B or T cells and internal Crbc control (dashed line); (2) free DXR; (3) non-targeted DXR-SL; and (4) DXR-SIL[anti-CD19].

pling of anti-CD19 on SIL retains the affinity of the free antibody [32]. The binding studies with ARH77 show that, compared with non-targeted liposomes, SIL[anti-CD19] rapidly and specifically associates with cells, even though the ARH77 cells express relatively low levels of CD19 binding sites. The relative K_D of the anti-CD19 mAb coupled to SIL was calculated as 2.2×10^{-3} μM, which is similar to that previously reported for a human B cell lymphoma cell line (1.8×10^{-3} μM) [32]. At maximal binding, approximately 5300 SIL[anti-CD19] or 1600 SL were bound per ARH77 cell. This translates into approximately 3700 specific SIL[anti-CD19] binding sites per ARH77 cell. The fact that equilibrium binding was not completely attained after 1 h at liposome concentrations of 1600 μmol PL/ml suggests that SIL[anti-CD19] bound to CD19 may be continually endocytosed and that the CD19 receptors recycle to the cell surface to participate in further binding.

When we compared the cytotoxicity of a leaky formulation of SIL[anti-CD19] with that of a non-leaky formulation, we observed higher cytotoxicity for the leaky formulation (DXR-PC40-SIL[anti-CD19]). The difference between DXR-PC40-SL and free drug is marginally significant at 24 h ($P<0.02$). Free drug is washed away after 1 h incubation, but the liposomal drug is still present in liposomes bound non-specifically to the cells. Leakage from the bound liposomes over 24 h appears to result in higher DXR levels in cells, hence the lower cytotoxicity compared with that of free DXR. This is also indirectly illustrated in Fig. 2b, in which PC40 liposomes show a two-fold higher relative mean fluorescence compared with HSPC liposomes, indicating higher non-specific absorption. Cytotoxicities of DXR-PC40-SIL and free drug are significantly different ($P<0.008$). DXR-PC40-SL and DXR-PC40-SIL both contained a low phase transition PL, PC40 [51].

Studies using free anti-CD19 to target B cell tumors have suggested that anti-CD19 signals a series of intracellular messages that lead to B cell differentiation, cell arrest or apoptosis [21,49,52]. We were unable to observe any effect of free anti-CD19 in our in vitro cytotoxicity assays using concentrations of up to 1 μM. In the cytotoxicity studies reported here, anti-CD19 did not induce any increased sensitivity of ARH77 cells to free DXR or liposomal DXR. In fact, at 1 h, free anti-CD19 in conjunction with targeted DXR-SIL[anti-CD19] competitively inhibited the action of DXR-SIL[anti-CD19], producing an IC_{50} equivalent to that of non-targeted liposomes. Although both anti-CD19 and DXR-SIL[anti-CD19] compete for the same membrane receptor, they may subsequently have cytotoxic effects via independent pathways, i.e. anti-CD19 signalling of apoptosis [21,49,52–54] versus DXR-induced DNA strand breaks in cells [55].

In myeloma PBMC, the exposure of cells to free DXR resulted in a non-selective cytotoxicity to both the B and T cell populations. However, immunoliposomal DXR was selectively cytotoxic to a large fraction of the B cells in MM blood, while leaving the T cells relatively unaffected (Fig. 7, Table 4). The ability of immunoliposomal DXR to selectively eradicate the circulating malignant B cell clone in vitro may have use in the treatment of MM in vivo. In this case, the pharmacokinetics of the liposomal drug carrier relative to the free drug may be advantageous. The rapid redistribution of free DXR ($t_{1/2} < 5$ min) following intravenous administration in humans leads to low plasma drug levels and hence to low cytotoxicity. Encapsulation of DXR in SL maintains steady DXR levels for several hours in circulation; the $t_{1/2}$ is approximately 48 h in humans [56]. We have previously shown in mice that the $t_{1/2}$ for SIL is similar to that for SL, suggesting that the SIL should have sufficient circulation times in humans to allow the liposomes to specifically bind to, and be taken up by, tumor cells.

P-gp associated with multidrug resistance is widely expressed in the B cells of MM patients [5,12,13]. Drugs like DXR, which are substrates for P-gp, are actively transported from P-gp-expressing cells, leading to low intracellular drug levels [5,57–59]. Our data show that the interaction of B cells with targeted DXR-SIL[anti-CD19] results in perinuclear, punctate DXR fluorescence throughout the cytoplasm. These observations are consistent with rapid cellular uptake of DXR-SIL[anti-CD19] by receptor-mediated endocytosis into endosomes [60–62]. Routing of a drug through receptor-mediated endocytosis may bypass the P-gp transporter, allowing eventual delivery of the drug to the nucleus [62], possibly explaining why the immunoliposomal DXR was effective against P-gp-expressing MM cells.

MM still remains largely incurable. Combination chemotherapy, radiotherapy and bone marrow transplants have resulted in limited therapeutic success [1,3,63]. Although these therapies are able to eliminate the plasma cells from the bone marrow, $CD19^+$ malignant B cells in the blood still persist after treatment and presumably have regenerative potential [4–6]. Relapse has been suggested to occur as these blood B cells continuously differentiate into end-stage plasma cells that migrate to the bone marrow [7,8]. Treatment with DXR-SIL[anti-CD19] may eradicate the malignant clone of circulating B cells, preventing these cells from repopulating the bone marrow and hence decreasing the likelihood of relapse. Although this treatment will also target normal B cells, in relapsed MM patients the vast majority of circulating B cells is derived from malignant clones. Presumably, normal B cells could be repopulated from end-stage plasma cells that do not express (or express low levels) of CD19 and would thus survive the immunoliposomal treatment.

This strategy is dependent on the extent to which the malignant B cells maintain surface expression of CD19 or other suitable target epitopes. Shedding or down-regulation of epitopes would limit this approach [17,20,29,52,64]. Highly expressed, stable, internalizing antigens like CD19 appear to be ideal target epitopes for such antibody-based therapies [17,19,52]. An attractive approach could be the use of a combination of several different immunoliposomes (including CD19 [26], CD20 [65], CD22 [66] and/or CD38) that would target both the malignant blood B cells and plasma cell components of this disease.

Acknowledgements

The editorial assistance of E. Moase and E. Street

is greatly appreciated. The authors would like to acknowledge the use of the Faculty of Medicine's Flow Cytometry and Confocal Microscopy Facilities. Ms. Eva Pruski assisted in preparation of monoclonal antibodies. This work is supported by grants from the Medical Research Council of Canada to T.M.A. and to L.M.P., and from SEQUUS Pharmaceuticals (now Alza Corporation), Menlo Park, CA, USA (T.M.A.).

References

[1] P.R. Griepp, Semin. Hematol. 29 (1992) 24–45.
[2] E.F. Osserman, M. Giampaolo, V.P. Butler, J. Am. Med. Assoc. 258 (1987) 2930–2937.
[3] B. Barlogie, G. Gahrton, Bone Marrow Transplant. 7 (1991) 71–79.
[4] A.J. Szczepek, P.L. Bergsagel, L. Axelsson, C.B. Brown, A.R. Belch, L.M. Pilarski, Blood 89 (1997) 1824–1833.
[5] L.M. Pilarski, A.J. Szczepek, A.R. Belch, Blood 90 (1997) 3751–3759.
[6] A.J. Szczepek, K. Seeberger, J. Wizniak, M.J. Mant, A.R. Belch, L.M. Pilarski, Blood 90 (1998) 2844–2855.
[7] L.M. Pilarski, A. Masellis-Smith, A. Szczepek, M.J. Mant, A.R. Belch, Leuk. Lymphoma 18 (1995) 179–187.
[8] L.M. Pilarski, G.S. Jensen, Hematol. Oncol. Clin. North Am. 6 (1992) 297–322.
[9] G.S. Jensen, A.R. Belch, M.J. Mant, B.A. Ruether, B.R. Yacyshyn, L.M. Pilarski, Am. J. Hematol. 43 (1992) 29–39.
[10] G.S. Jensen, M.J. Mant, A.R. Belch, J.R. Berensen, B.A. Ruether, L.M. Pilarski, Blood 78 (1991) 711–719.
[11] A. Masellis-Smith, A.R. Belch, M.J. Mant, L.M. Pilarski, Cancer Res. 57 (1997) 930–936.
[12] L.M. Pilarski, C.E. Cass, T. Tsuro, A.R. Belch, Curr. Top. Microbiol. Immunol. 182 (1992) 177–185.
[13] L.M. Pilarski, A.R. Belch, Blood 83 (1994) 724–736.
[14] L.M. Pilarski, A.R. Belch, Leuk. Lymphoma 17 (1995) 367–374.
[15] T.M. Grogan, C.M. Spier, S.E. Salmon, M. Matzner, J. Rybski, R.S. Weinstein, R.J. Scheper, W.S. Dalton, Blood 81 (1993) 490–495.
[16] Y.V.J.M. van Oosterhout, I.E. van den Herik-Oudijk, H.M.C. Wessels, T. de Witte, J.G.J. van de Winkel, F.W.M.B. Preijers, Cancer Res. 54 (1994) 3527–3532.
[17] F.M. Uckun, W. Jaszcz, J.L. Ambrus, A.S. Fauci, K. Gajl-Peczalska, S.W. Song, M.R. Wick, D.E. Myers, K. Waddick, J.A. Ledbetter, Blood 71 (1988) 13–29.
[18] I.C. Nicholson, K.A. Lenton, D.J. Little, T. DeCorso, F.T. Lee, A.M. Scott, H. Zola, A.W. Hohmann, Mol. Immunol. 34 (1998) 1157–1165.
[19] M.A. de Rie, T.N. Schumacher, G.M. van Schijndel, R.A. van Lier, F. Miedema, Cell. Immunol. 118 (1989) 368–381.
[20] O.W. Press, A.G. Farr, K.I. Borroz, S.K. Andersen, P.J. Martin, Cancer Res. 49 (1989) 4906–4912.
[21] M.A. Ghetie, L.J. Picker, J.A. Richardson, K. Tucker, J.W. Uhr, E.S. Vitetta, Blood 83 (1994) 1329–1336.
[22] B.L. Pizer, J.T. Kemshead, Leuk. Lymphoma 15 (1994) 281–289.
[23] S.F. Vervoordeldonk, P.A. Merle, E.F. van Leeuwen, A.E. von dem Borne, I.C. Slaper-Cortenbach, Cancer 73 (1994) 1006–1011.
[24] M.J. Stone, E.A. Sausville, J.W. Fay, D. Headlee, R.H. Collins, W.D. Figg, M. Stetler Stevenson, V. Jain, E.S. Jaffe, D. Solomon, R.M. Lush, A. Senderowicz, V. Ghetie, J. Schindler, J.W. Uhr, E.S. Vitetta, Blood 88 (1996) 1188–1197.
[25] A. Hekman, A. Honselaar, W.M. Vuist, J.J. Sein, S. Rodenhuis, W.W. Bokkel Huinink, R. Somers, P. Rumke, C.J. Melief, Cancer Immunol. Immunother. 32 (1991) 364–372.
[26] M.L. Grossbard, A.S. Freedman, J. Ritz, F. Coral, V.S. Goldmacher, L. Eliseo, N. Spector, K. Dear, J.M. Lambert, W.A. Blattler, J.A. Taylor, L.M. Nadler, Blood 79 (1992) 576–585.
[27] T.M. Allen, I. Ahmad, D.E. Lopes de Menezes, E.H. Moase, Biochem. Soc. Trans. 23 (1995) 1073–1079.
[28] M.H. Vingerhoeds, G. Storm, D.J. Crommelin, Immunomethods 4 (1994) 259–272.
[29] J.W. Park, K. Hong, D.B. Kirpotin, D. Papahadjopoulos, C.C. Benz, Adv. Pharmacol. 40 (1997) 399–435.
[30] I. Ahmad, M. Longenecker, J. Samuel, T.M. Allen, Cancer Res. 53 (1993) 1484–1488.
[31] A. Mori, S.I. Kennel, M.V.B. Waalkes, G.L. Scherphof, L. Huang, Cancer Chemother. Pharmacol. 35 (1995) 447–456.
[32] D.E. Lopes de Menezes, L.M. Pilarski, T.M. Allen, Cancer Res. 58 (1998) 3320–3330.
[33] J. Lang, C. Vigo-Pelfrey, F. Martin, Chem. Phys. Lipids 53 (1990) 91–101.
[34] T.M. Allen, C.B. Hansen, F. Martin, C. Redemann, A. Yau-Young, Biochim. Biophys. Acta 1066 (1991) 29–36.
[35] S. Zalipsky, Bioconjug. Chem. 4 (1993) 296–299.
[36] H. Zola, P.J. Macardle, T. Bradford, H. Weedon, H. Yasui, Y. Kurosawa, Immunol. Cell Biol. 69 (1991) 411–422.
[37] G.L. Pool, M.E. French, R.A. Edwards, L. Huang, R.H. Lumb, Lipids 17 (1982) 445–452.
[38] J.T. Derksen, H.W. Morselt, G.L. Scherphof, Biochim. Biophys. Acta 931 (1987) 33–40.
[39] L.D. Mayer, M.J. Hope, P.R. Cullis, Biochim. Biophys. Acta 858 (1986) 161–168.
[40] G.R. Bartlett, J. Biol. Chem. 234 (1959) 466–468.
[41] D.D. Lasic, Liposomes: from Physics to Applications, Elsevier Science Publishers, Amsterdam, 1993.
[42] E.M. Bolotin, R. Cohen, L.K. Bar, S.N. Emanuel, D.D. Lasic, Y. Barenholz, J. Liposome Res. 4 (1994) 455–479.
[43] C.B. Hansen, G.Y. Kao, E.H. Moase, S. Zalipsky, T.M. Allen, Biochim. Biophys. Acta 1239 (1995) 133–144.
[44] D.L. Daleke, K. Hong, D. Papahadjopoulos, Biochim. Biophys. Acta 1024 (1990) 352–366.

[45] R.M. Straubinger, D. Papahadjopoulos, K. Hong, Biochemistry 29 (1990) 4929–4939.
[46] T. Mosmann, J. Immunol. Methods 65 (1983) 55–63.
[47] A.W. Coleman, M.J. Maguire, J.R. Coleman, J. Histochem. Cytochem. 29 (1981) 959–968.
[48] D.W. Hedley, M.L. Friedlander, I.W. Taylor, Cytometry 6 (1985) 327–333.
[49] A.C. Goulet, V.S. Goldmacher, J.M. Lambert, C. Baron, D.C. Roy, E. Kouassi, Blood 90 (1997) 2364–2375.
[50] J.M. Lambert, V.S. Goldmacher, A.R. Collinson, L.M. Nadler, W.A. Blattler, Cancer Res. 51 (1991) 6236–6242.
[51] T.M. Allen, D. Stuart, in: A.S. Janoff (Ed.), Liposomes: Rational Design, Marcel Dekker, New York, 1998, pp. 63–97.
[52] E.S. Vitetta, J.W. Uhr, Cancer Res. 54 (1994) 5301–5309.
[53] M. Bruggemann, G.T. Williams, C.I. Bindon, M.K. Clark, M.R. Walker, R. Jefferis, H. Waldmann, M.S. Neugerger, J. Exp. Med. 166 (1987) 127–142.
[54] Z. Steplewski, L.K. Sun, C.W. Shearman, J. Ghrayeb, P. Daddona, H. Koprowski, Proc. Natl. Acad. Sci. USA 85 (1988) 4852–4856.
[55] L. Gianni, B. Corden, C. Myers, Rev. Biochem. Toxicol. 5 (1983) 1–82.
[56] D.W. Northfelt, F.J. Martin, L.D. Kaplan, J. Russell, M. Andersen, J. Lang, P.A. Volberding, Proc. Am. Soc. Clin. Oncol. 12 (1993) A8.
[57] M.M. Gottesman, Cancer Res. 53 (1993) 747–754.
[58] G. Bradley, V. Ling, Cancer Metastasis Rev. 13 (1994) 223–233.
[59] T. Sumizawa, Y. Chuman, H. Sakamoto, K. Iemura, K.C. Almquist, R.G. Deeley, S.P. Cole, S. Akiyama, Somat. Cell Mol. Genet. 20 (1994) 423–435.
[60] R.J. Lee, P.S. Low, J. Biol. Chem. 269 (1994) 3198–3204.
[61] D. Kirpotin, J.W. Park, K. Hong, S. Zalipsky, W.-L. Li, P. Carter, C.C. Benz, D. Papahadjopoulos, Biochemistry 36 (1997) 66–75.
[62] D.E. Lopes de Menezes, M.J. Kirchmeier, J.-F. Gagne, L.M. Pilarski, T.M. Allen, J. Liposome Res. 9 (1999) 199–228.
[63] D.E. Bergsagel, Ann. Rev. Med. 30 (1979) 431–433.
[64] T.M. Allen, C.B. Hansen, D.D. Stuart, in: D.D. Lasic, D. Papahadjopoulos (Eds.), Medical Applications of Liposomes, Elsevier Science Publishers, Amsterdam, 1998, pp. 297–323.
[65] M.S. Kaminski, K.R. Zasadny, I.R. Francis, A.W. Milik, C.W. Ross, S.D. Moon, S.M. Crawford, J.M. Burgess, N.A. Petry, G.M. Butchko, S.D. Glenn, R.L. Wahl, N. Engl. J. Med. 329 (1993) 459–465.
[66] E.S. Vitetta, E. Stone, P. Amlot, J. Fay, R. May, M. Till, J. Newman, P. Clark, R. Collins, D. Cunningham, V. Ghetie, J.W. Uhr, P.E. Thorpe, Cancer Res. 51 (1991) 4052.